Experimental Characterization of Unsteady Forces Triggered by Cavitation on a Centrifugal Pump

Dario Valentini, Giovanni Pace, Angelo Pasini, Ruzbeh Hadavandi, Luca D'agostino

Experimental Characterization of Unsteady Forces Triggered by Cavitation on a Centrifugal Pump

Dario Valentini[1]*, Giovanni Pace[1], Angelo Pasini[2], Ruzbeh Hadavandi[1], Luca d'Agostino[2]

ISROMAC 2017

International Symposium on Transport Phenomena and Dynamics of Rotating Machinery

Hawaii, Maui

December 16-21 2017

Abstract

The paper presents an experimental campaign aimed at the characterization of the relationship between cavitation-induced instabilities and forces acting on the shaft relevant to space application turbopumps. The experiments have been carried-out on a 6-bladed, unshrouded centrifugal turbopump. The described apparatus allows for contemporary measurements of the flow instabilities and the force exchanged between the impeller and the shaft. Pressure fluctuations are frequency analyzed allowing for understanding the instability nature (axial, rotating) and their main characteristics (e.g. amplitude, rotating direction). The frequency content of the force components highlights a strong relationship of the z-component (along the rotating axis) with axial instabilities. On the other hand, rotating cavitation may involve force oscillations along all the three components leading to unwanted and dangerous fluctuating unbalances perpendicular to the rotating axis.

Keywords

Cavitation — Rotordynamic — Centrifugal Pump

[1] *Chemical Propulsion, SITAEL S.p.A., Pisa, Italy*

[2] *Department of Civil and Industrial Engineering, University of Pisa, Pisa, Italy*

*__Corresponding author__: dario.valentini@sitael.com

INTRODUCTION

Propellant feed turbopumps are a crucial component of all liquid propellant rocket engines due to the severe limitations associated with the design of dynamically stable, high power density machines capable of meeting the extremely demanding suction, pumping and reliability requirements of modern STSs (Space Transportation Systems).

The attainment of such high power/weight ratios is invariably obtained by running the impeller at the maximum allowable speed and low shaft torque. Current configurations in space applications are typically characterized by the presence of lighter, but also more flexible, shafts. Therefore, since the operation under cavitating conditions is tolerated, the turbopump is exposed to the onset of dangerous fluid dynamic and rotordynamic instabilities which may be triggered by cavitation phenomena. When designing a turbomachine, particularly if it has to operate at high rotational speeds, it is important to be able to predict the fluid-induced forces acting on the various components of the machine. The study of radial and rotordynamic forces on turbomachines components, by means of analytical/numerical and experimental approaches has been extensively carried out in the last 50 years by many researchers all around the world, as in the following refs. [1-7]. However, the experimental characterization of the influence of cavitation on these phenomena is still very poor even if it is a common operational condition in space application. Moreover, it is extremely important since the occurrence of cavitation drastically modifies the inertia of the fluid surrounding the impellers and, in turn, the critical speeds of the machine.

Fluid instabilities that develop in space inducers have been widely studied in the past, such in the following sources: [9-17]. However, a lack in centrifugal pumps experimental activities does not allow a complete understanding of the cavitation induced flow phenomena. In fact, few detailed experimental results can be found in literature, analyzing the instabilities and their interaction with the system even if rotating cavitation [18] and auto-oscillation [19] have been detected and studied in previous works.

The experimental characterization of the unsteady fluid forces/moments acting on space turbopump impellers as a consequence of the onset of the most dangerous types of cavitation-induced instabilities is here described and analyzed.

This is done by employing a new methodology, consisting in measuring simultaneously the forces acting on the shaft by means of a rotating dynamometer previously employed in past experimental activities [20-22] and the pressure field around the centrifugal pump at different locations by means of piezo-electric pressure transducers This technique allows for comparing and evaluating the influence of pressure fluctuations on the unsteady force component that the pump exerts on the shaft, making possible to relate the nature of the unsteady flow phenomena interacting with the system by means of mechanical stresses.

1 ANALYSIS AND EXPERIMENTAL SETUP

1.1 Experimental apparatus

Figure 1 shows the general layout of the Cavitating Pump Rotordynamic Test Facility (CPRTF, see [23] for further information) at SITAEL S.p.A. (formerly ALTA S.p.A.). The facility is specifically intended for the experimental analysis of the relevant phenomena on space application turbopumps with particular attention on cavitation-related phenomena.

In order to relate the fluid instabilities with the unsteady forces acting on the pump, the experiments have been carried out by jointly using a rotating dynamometer (extensively used in past experimental activities, [24]), and a suitable number of piezoelectric pressure transducers (PCB Piezotronics, mod. S112A22) flush-mounted on the machine casing. The dynamometer has been placed downstream of the supports, between the pump and the rotor shaft, in order to avoid the influence of seals and bearing forces. The positions of the pressure transducers have been chosen in order to evaluate and identify the nature of the fluid instability (rotational/axial), thus different axial and azimuthal positions have been exploited. For this purpose, three different axial positions have been made available for the transducers on the pump casing (Figure 2 and Figure 4): upstream, midstream, and downstream (at the diffuser). With reference to Figure 4, the relative positions of the pressure taps have been designed in such a way that, at the same instant, number-like taps should face the through-flow of the same blade channel. The taps exploited during the present campaign are:

Table 1. Pressure taps exploited for the present campaign.

Position	Tap
Upstream	1, 2, 3, 4
Midstream	1,7
Downstream	1,2,3,7

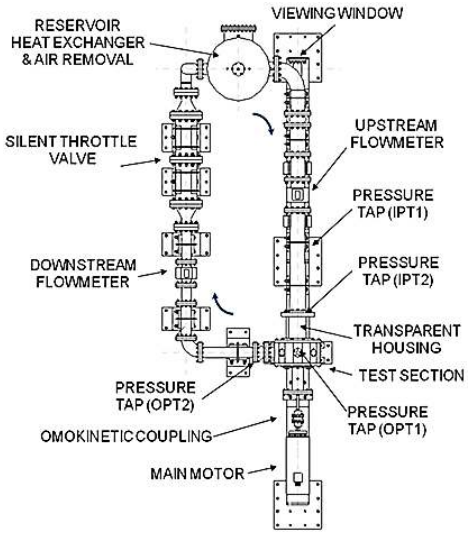

Figure 1. The CPRTF lay-out in SITAEL S.p.A.

With reference to Figure 1 and Figure 2, the test setup includes:

- two electromagnetic flowmeters (Fisher-Rosemount, model 8732E, range: 0-100 l/s, accuracy 0.5% FS), for the measurement of the inlet and outlet flow rates;
- an absolute pressure transducer ($p_{in}@IPT1$) placed 6 diameters upstream w.r.t. the blade leading edge (GE, model Druck PMP1400, range 0÷1 bar, accuracy 0.25% FS) for the assessment of the inlet cavitation number (σ);
- an absolute pressure transducer ($p_C@OPT1$) placed in the test chamber/section in order to measure the influence of the pressure on the axial force measured by the dynamometer. Indeed, there is a measured force related only to the pressure difference between the water pressure and the sealed dynamometer inside which is at atmospheric condition (GE, model UNIK5000, range 0÷6 bar, accuracy 0.1% FS);
- one differential pressure transducer ($\Delta p\ @IPT1\ to\ OPT2$) which measures the pump pressure rise between the inlet station placed at 6 diameters upstream the blade leading edge and outlet station placed about two diameters downstream the blade trailing edge (GE, model UNIK5000, range 0÷5 bar, accuracy 0.1% FS);
- one temperature sensor PT100 (range 0÷100 °C, accuracy 0.5°C).

The test item employed in the present experimental campaign has been designed at SITAEL and it is a six-bladed radial pump (Figure 3) whose main characteristics are summarized in Table 2. The design is based on the reduced order model developed at ALTA S.p.A. [25, 26] which has been already applied to a similar radial impeller [27]. The clearance between the impeller and the casing is equal to 1 mm.

Table 2. Most relevant geometrical and operational parameters of the VAMPUFF pump.

Design flow coefficient @ r_2	[--]	Φ_D	0.120
Number of blades	[--]	N	6
Outlet radius	$[mm]$	r_2	105.00
Inlet tip radius	$[mm]$	r_{T1}	55.50
Inlet hub radius	$[mm]$	r_{H1}	31.42
Axial length	$[mm]$	z_{H2}	67.00
Inlet tip blade angle	$[deg]$	γ_{T1}	47.70
Inlet backsweep angle	$[deg]$	χ_1	0
Diffuser outlet radius	$[mm]$	r_3	126
Design Rotating Speed	$[rad/s]$ ($[rpm]$)	Ω	1500 (1500)
Design volumetric flowrate	$[m^3/s]$	Q_{des}	0.022
Mean blade height	$[mm]$		18.84
Tip solidity	[--]	σ_T	2.64
Incidence tip angle @ design	$[deg]$	α	18.90
Outlet tip blade mean angle	$[deg]$	γ_{T2}	89.94
Outlet tip backsweep angle	$[deg]$	χ_2	64.00

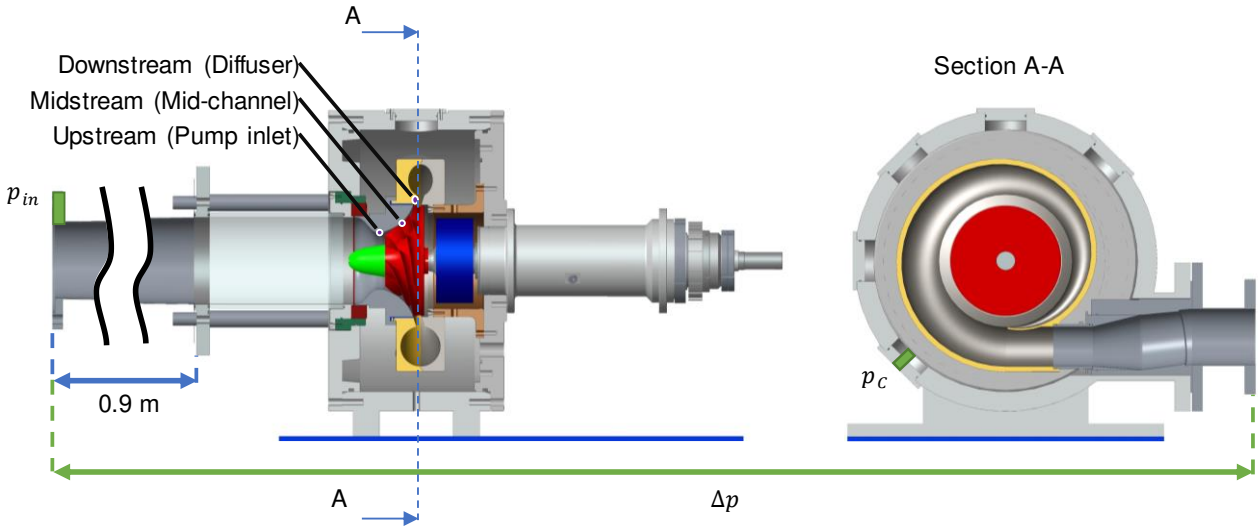

Figure 2. VAMPUFF test setup.

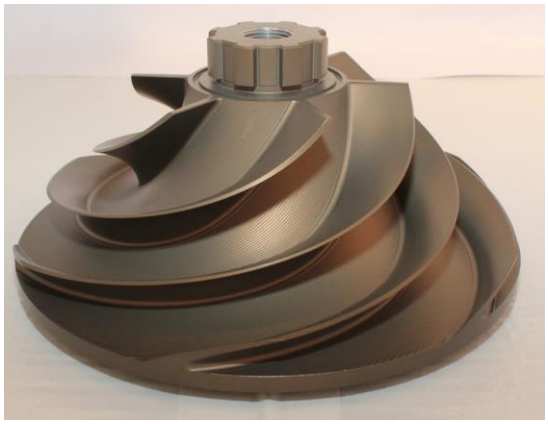

Figure 3. VAMPUFF radial impeller.

1.1 Pumping Performance

The tests are performed at room temperature ($T \cong 20°C$), while the inlet pressure is set well above the vapor pressure in order to avoid cavitation inception within the pump. Referring to the pump geometric in Table 2, the parameters used to characterize the performance are:

Total Head Coefficient	$\Psi_T = \Delta p_T / \rho\, \Omega^2 r_2^2$
Flow Coefficient	$\Phi = Q / \Omega r_2^3$
Reynold Number	$Re = 2\Omega r_2^2 / \nu$

1.2 Cavitating Performance

Steady-state cavitating experiments are performed by maintaining a fixed inlet pressure condition during the experiment. Continuous cavitating experiments are performed by slowly lowering the inlet pressure in order to reach different cavitating regimes. The acquired signals of each continuous experiment are divided into sub-blocks where the operating conditions and relevant phenomena do not change significantly. The main parameters used to characterize the cavitating performance are:

Head Coefficient	$\Psi = \Delta p / \rho\, \Omega^2 r_2^2$
Cavitation Number	$\sigma = (p_{in} - p_v) / 0.5 \rho \Omega^2 r_2^2$

1.3 Flow Instabilities and Unsteady Fluid Forces

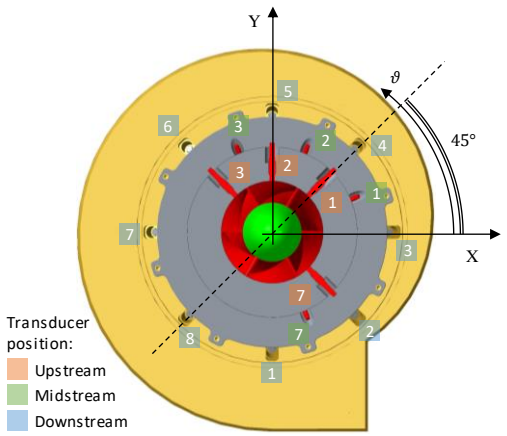

Figure 4. Piezoelectric pressure transducers positions.

The pressure fluctuations of the flow through the pump triggered or not by cavitation have been investigated during the cavitating experiments. Cervone, et al., and d'Agostino, et al. [16, 28] report the procedures already exploited by the authors and here just summarized. As for the cavitating performance evaluation, the signals acquired by means of the piezoelectric transducers located on the pump casing and diffuser are divided into sub-blocks. Per each sub-block, the signals are fast-Fourier transformed in order to obtain the frequency content of oscillating phenomena. At each frequency of interest, the analysis of the cross-spectrum phase of signals from transducers placed at the same axial location but at different azimuthal positions allows for understanding the physical nature of the phenomenon. In fact, oscillating axial phenomena involve signals characterized by zero-phase cross-spectrum. On the other hand, rotating phenomena lead to cross-spectrum phases (φ) proportional to the circumferential spacing $\Delta\vartheta$ between transducers and proportional to the phenomenon number of lobes (n). For instance, for a generic cross-spectrum from the transducer "1" to the transducer "2", it would be:

$$n = |\varphi_{12}/(\vartheta_2 - \vartheta_1)|$$

where negative values of φ_{12} imply a phenomenon moving from transducer "1" to transducer "2". Aliasing in the azimuthal direction is eliminated by comparison of the cross-correlations of pressure signals from transducers with different angular separations. The analysis is validated based on the value of the coherence function between signals obtained from two generic transducers (x, y) $\gamma_{xy} = |S_{xy}(f)|^2/[S_{xx}(f)S_{yy}(f)]$, where S is either the cross-spectrum or the auto-spectrum of the referred transducers (x, y) in the subscripts (see [29] for further information). Here, only phenomena with values of γ_{xy} greater than 0.95 have been considered.

In order to understand the frequency content of the signals recorded through the dynamometer, it is useful to consider and compare the effect of different types of unsteady forces on the dynamometer rotating frame (xyz) and on the absolute fixed one (XYZ), where z and Z are directed along the rotating axis. Therefore, the force evaluated in the two reference frames has the same z-component as well as the same total force acting on the plane $\mathrm{X} - \mathrm{Y}$ $(x - y)$.

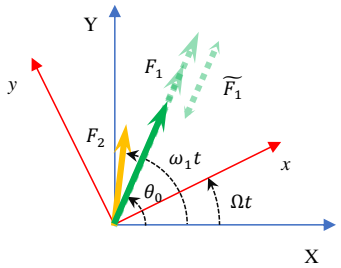

Figure 5. Schematic of a generic unsteady force acting on the shaft w.r.t. the rotating frame and the fixed one.

Considering Figure 5, the schematic proposed involves a fluctuating phenomenon generating a force with constant direction (θ_0) w.r.t. the fixed reference frame, a mean value F_0 and an oscillating amplitude: $F_1 = F_0 + \tilde{F_1}\, cos(\omega_2 t)$. Furthermore, the schematic considers a constant amplitude force F_2 rotating w.r.t. the fixed reference frame with an angular velocity ω_1. The force components in the rotating frame and in the fixed one are:

$$F_X = F_0\, cos(\theta_0) + \tilde{F}_1\, cos(\omega_2 t)\, cos(\theta_0) + F_2 cos(\omega_1 t)$$

$$F_Y = F_0\, sin(\theta_0) + \tilde{F}_1\, cos(\omega_2 t)\, sin(\theta_0) + F_2 sin(\omega_1 t)$$

$$F_x = \frac{\tilde{F}_1}{2}\cos[(\omega_2 - \Omega)t + \theta_0] + \frac{\tilde{F}_1}{2}\cos[(\omega_2 + \Omega)t - \theta_0] + F_2 cos[(\omega_1 - \Omega)t] + F_0\, cos(\Omega t - \theta_0)$$

$$F_y = \frac{\tilde{F}_1}{2}\sin[(\omega_2 - \Omega)t + \theta_0] - \frac{\tilde{F}_1}{2}\sin[(\omega_2 + \Omega)t - \theta_0] + F_2 sin[(\omega_1 - \Omega)t] - F_0\, sin(\Omega \mathrm{t} - \theta_0)$$

Therefore, a frequency analysis of the force components would show 2 frequencies (ω_1, ω_2) in the fixed reference frame. On the other hand, the same analysis in the rotating frame would show multiple frequencies shifted from the above-mentioned ones by $\pm\Omega$.

2 RESULTS AND DISCUSSION

2.1 Pumping Performance

Figure 6 shows the pumping performance obtained at three different rotating speeds. The data overlapping confirms the Reynolds independence of the tests (fully turbulent flow).

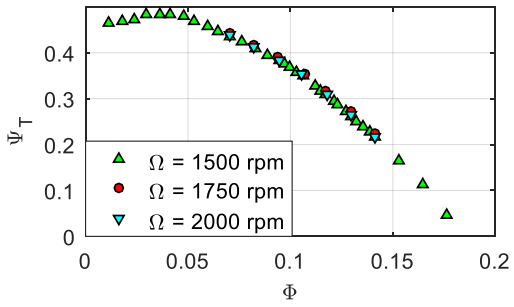

Figure 6. VAMPUFF pumping performance, $T \cong 20°C$.

2.2 Cavitating Performance

Figure 7 reports the VAMPUFF cavitating performance obtained at different flow coefficients Φ. Per each flow coefficient, solid markers with black borders show results obtained from steady-state experiments, while blank markers report continuous experiments results. The overlapping of the data from the two different procedures confirms the goodness of the continuous data which can reliably represent the cavitating performance. The rotational speed $\Omega = 1750$ rpm allows for measurable cavitation and forces without exceeding the maximum capability of the dynamometer.

Table 3. Relevant parameters for the cavitating experiments.

Sampling Frequency (f_s)	$5000\ Hz$
Temperature	$20\ °C$
Experiment Duration (cont.)	$240\ s$

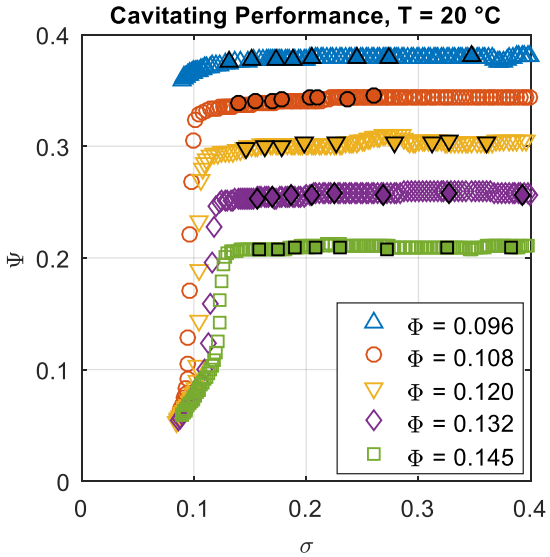

Figure 7. VAMPUFF cavitating performance at different flowrates $(T = 20°C;\ \Omega = 1750\ rpm)$.

2.3 Flow Instabilities and Unsteady Fluid Forces

The systematic evaluation of the flow instabilities during the cavitating experiments highlighted the presence of rotating and axial phenomena for different flowrates, as briefly summarized in Table 4. In the table, at the same flowrate, oscillating phenomena showing analogous characteristics (rotating with 1 lobe, axial, etc.) are grouped together regardless the operating regimes (σ, frequency).

Table 4. Identified phenomena at different flowrates.

Φ (Φ/Φ_D)	Identified Phenomena
0.096 (0.8)	Rotating (1 lobe and 2 lobes); axial
0.108 (0.9)	Rotating (1 lobe and 2 lobes); axial
0.120 (1.0)	Rotating (1 lobe); axial
0.132 (1.1)	Rotating (1 lobe); axial
0.144 (1.2)	Axial

The presence of cavitation instabilities leads to unwanted forces on the shaft even at $\Phi = \Phi_D$. However, at design condition the intensity of the detected oscillating forces is minor than at lower flowrates. For this reason, the present study only focuses on $\Phi = 0.108$ $(\Phi/\Phi_D = 0.9)$ in order to show some of the typical pressure-force spectra relationships found at all the tested regimes.

Figure 8 reports the cavitating performance at a nominal $\Phi_N = 0.108$ as well as the flow coefficient behavior during the inlet pressure decay. At the end of the experiment the massive presence of cavitation leads to the breakdown which, in turn, leads to the flow coefficient drop.

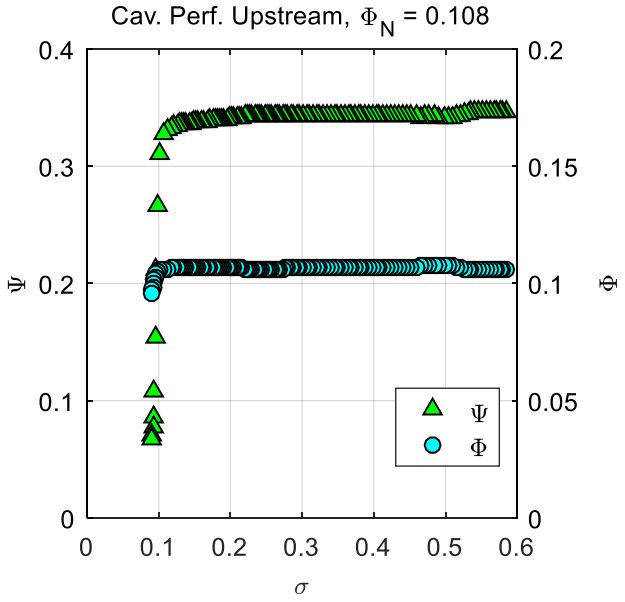

Figure 8. Cavitating performance and the flow coefficient evolution, nominal $\Phi_N = 0.108$ $(90\%\Phi_D)$.

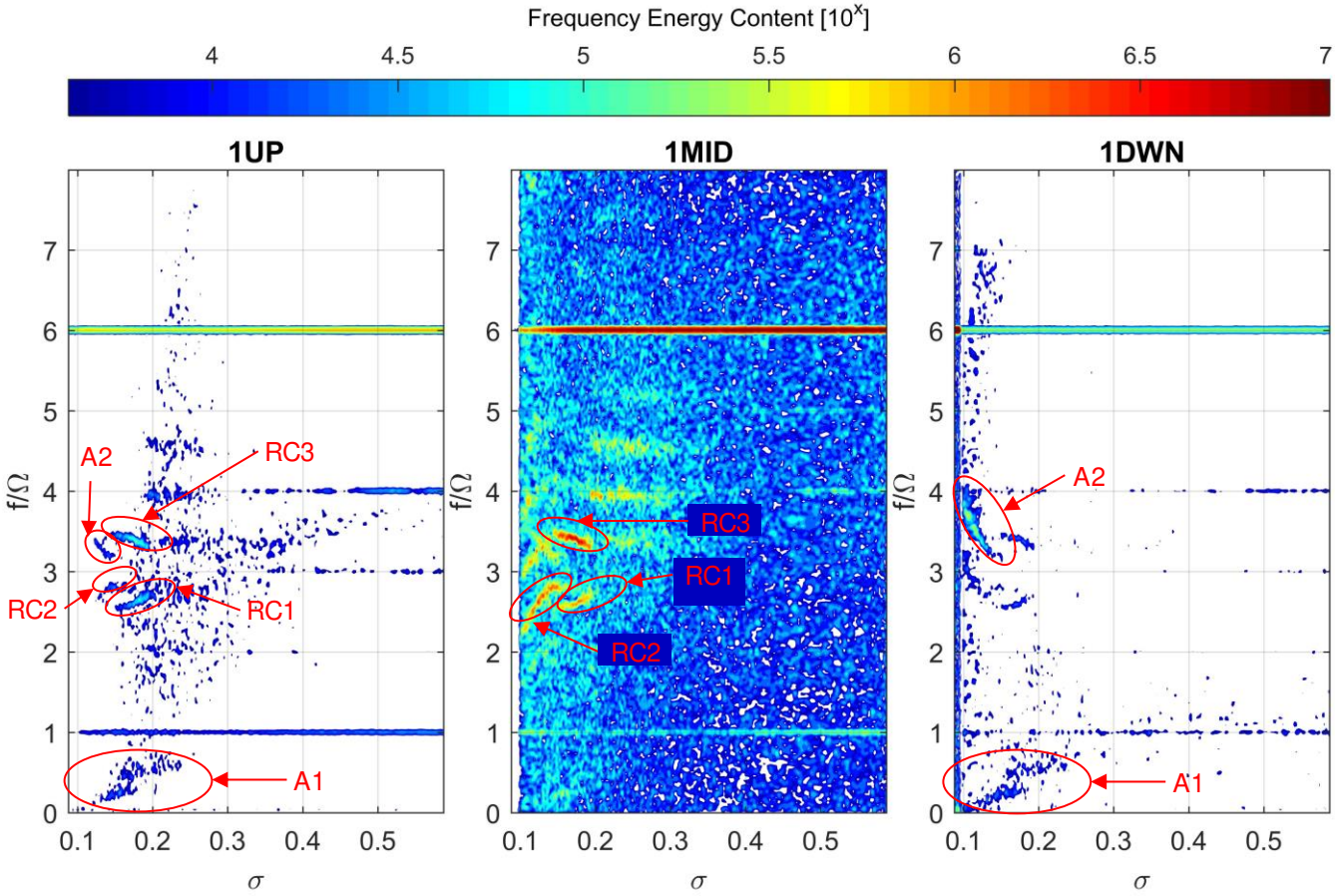

Figure 9. Frequency energy content $[Pa^2 \cdot s]$ of pressure transducers placed upstream (left), midstream (center), and downstream (right).

The flow instabilities illustrated in this paper are basically connected with the presence of cavitation. According to [30], cavitation inception usually starts in the tip vortex generated at the blade inlet. Therefore, it is of no surprise that the major part of the found phenomena is clearly visible by the upstream pressure transducers, becoming less visible while moving downstream. On the other hand, axial phenomena effectively propagate from the upstream to the downstream and vice versa becoming clearly visible in both stations.

Figure 9 reports the energy frequency content of three pressure transducers as representative of the three different stream locations: upstream, midstream, and downstream (according to Figure 2 and Figure 4) versus the cavitation number σ. Per each frequency, the frequency energy content (E_f) is directly related to the amplitude (A_f) of the acting oscillating phenomenon as follows:

$$E_f = \frac{A_f^2}{4}\frac{N_s}{f_s}$$

where N_s is the number of samples considered for the FFT while f_s is the sampling frequency exploited during the experiment.

While the blade passage frequency is clearly visible at 6Ω per each station, the other relevant phenomena are generally of major interest at a single station. In order to understand the physical nature of such oscillating phenomena, Figure 10, Figure 11, and Figure 12 report the phase of the cross-spectrum of the upstream, midstream, and downstream pressure transducers, respectively. The figures show only the phenomena of major interest characterized by an amplitude $A_f \geq 100\ Pa$ and a coherence $\gamma_{xy} \geq 0.95$, focusing on the range of $f/\Omega = 0 \div 4$ where interesting phenomena have been found. The phase values allow for understanding the nature of the phenomenon [28, 31]. The main outcomes of this analysis are summarized in Table 5.

Table 5. Summary of the found instabilities at $\Phi_N = 0.108$.

ID	Freq. Range f/Ω $(f\ [Hz])$	σ range	Characteristics	Major Station
A1	0.38 - 0.1 (11 - 3)	0.16 - 0.12	Axial	Up
RC1	2.74 - 2.57 (80 - 75)	0.2 - 0.16	Rotating 1 lobe	Up
RC2	2.85 - 2.33 (83 - 68)	0.16 - 0.11	Rotating 2 lobes	Mid
A2	3.22 - 3.81 (94 - 111)	0.16 - 0.10	Axial	Down
RC3	3.26 - 3.46 (95 - 101)	0.19 - 0.14	Rotating 1 lobe	Mid

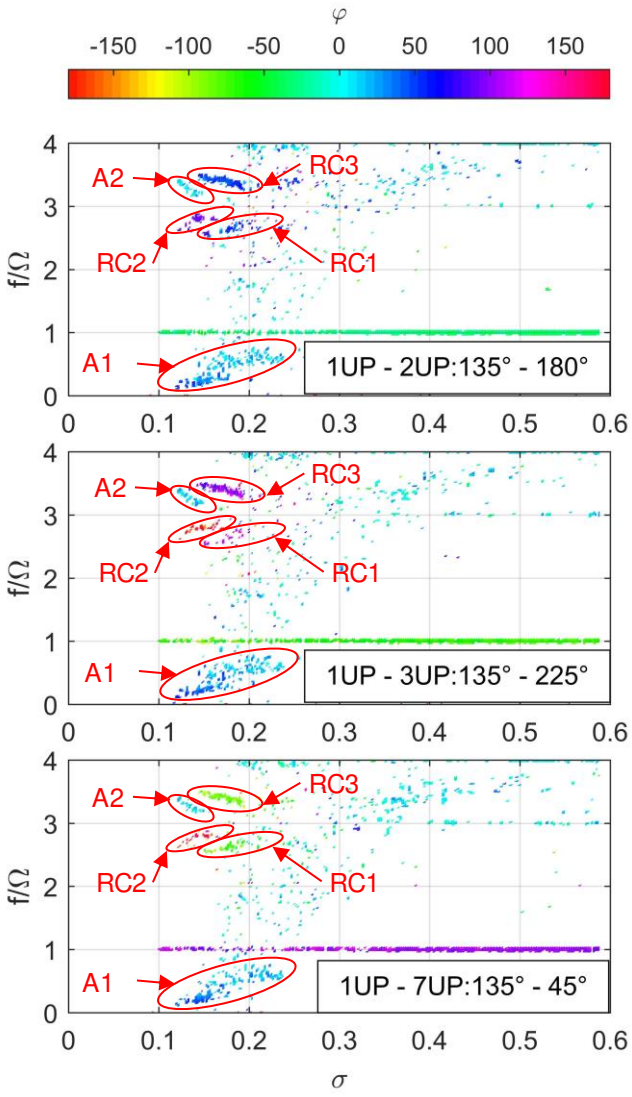

Figure 10. Cross-spectrum phase of the upstream pressure transducers, $\Phi = 0.108\ (90\%\Phi_D)$.

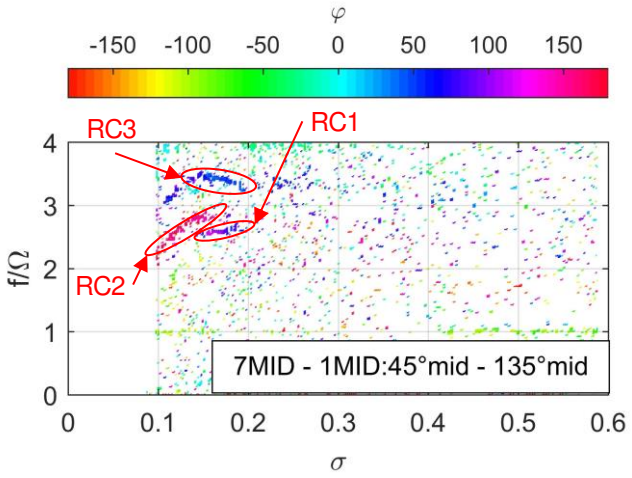

Figure 11. Cross-spectrum phase of the midstream pressure transducers, $\Phi = 0.108\ (90\%\Phi_D)$.

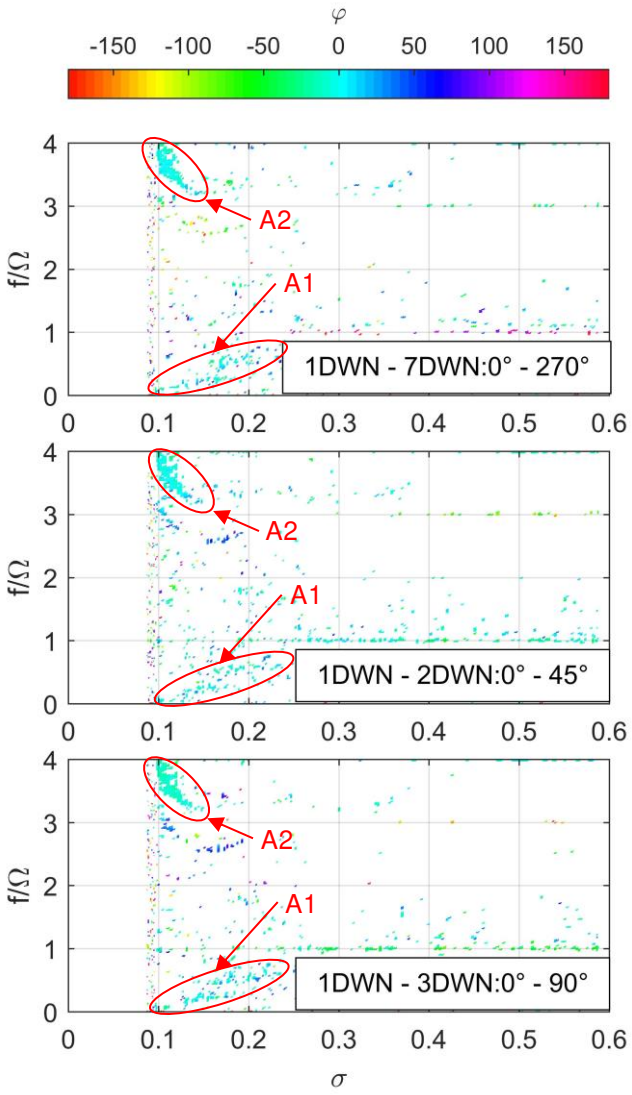

Figure 12. Cross-spectrum phase of the downstream pressure transducers, $\Phi = 0.108\ (90\%\Phi_D)$.

Figure 13 shows the frequency energy content of the force components measured by the dynamometer with a force amplitude oscillation greater than $0.5\ N$. In particular, the figure reports the force components independent of the chosen reference frame (i.e. rotating or fixed), as described previously.

RC2 and RC3 do not generate relevant effects on the forces sensed by the dynamometer, therefore they won't be further discussed. On the contrary, some of the instabilities reported in Table 5 clearly lead to unwanted oscillations of the force acting on the shaft. In particular, the two axial instabilities A1 and A2 generate oscillations of F_z for corresponding values of $\sigma - f$, while they are not visible at all on a plane perpendicular to the rotational axis (XY, xy).

Like A1 and A2, the pressure distribution connected with the rotating cavitation-induced instability RC1 generates a fluctuating component on the rotational axis.

However, RC1 also leads to a fluctuating component on the plane $\mathrm{XY}\ (xy)$ at the same operating regimes (σ) and frequencies, and with an intensity directly connected to the corresponding energy value.

In order to understand the RC1 effects on the plane $\mathrm{XY}\ (xy)$, it is useful to analyze the frequency content of the force component F_X and F_x defined in the fixed frame and in the rotating one, respectively (Figure 14). Let's consider the schematic proposed in Figure 5 and in the following. The frequency energy content of F_{xy} is influenced only by the amplitude and the acting frequency of $\tilde{F}_1$. The pressure distribution due to the presence of cavitation in the form of RC1 generates a rotating force imbalance with a rotational velocity corresponding to the rotational velocity of the phenomenon itself, which is given by the pressure transducer analysis. Moreover, when this pressure distribution interacts with the (static) volute tongue at the impeller exit, it may lead to an oscillating unbalanced force at the same frequency as the phenomenon itself. The above considerations may be summarized as $\omega_2 = \omega_1 = 2\pi f_{RC1}$, therefore:

$$F_X = F_0\, cos(\theta_0) + [\tilde{F}_1\, cos(\theta_0) + F_2] cos(\omega_1 t)$$

which is coherent with the frequency content in Figure 14. Moreover, the corresponding force on the rotating frame is given by:

$$F_x = \frac{\tilde{F}_1}{2}\cos[(\omega_1 - \Omega)t + \theta_0] + F_2 cos[(\omega_1 - \Omega)t] + \frac{\tilde{F}_1}{2}\cos[(\omega_1 + \Omega)t - \theta_0] + F_0\, cos(\Omega t - \theta_0)$$

where there are only three acting frequencies (as shown in Figure 14, center):

1. $(\omega_1 - \Omega)/2\pi$, whose intensity depends on the combination of $\tilde{F}_1, F_2, \theta_0$;
2. $(\omega_1 + \Omega)/2\pi$;
3. Ω.

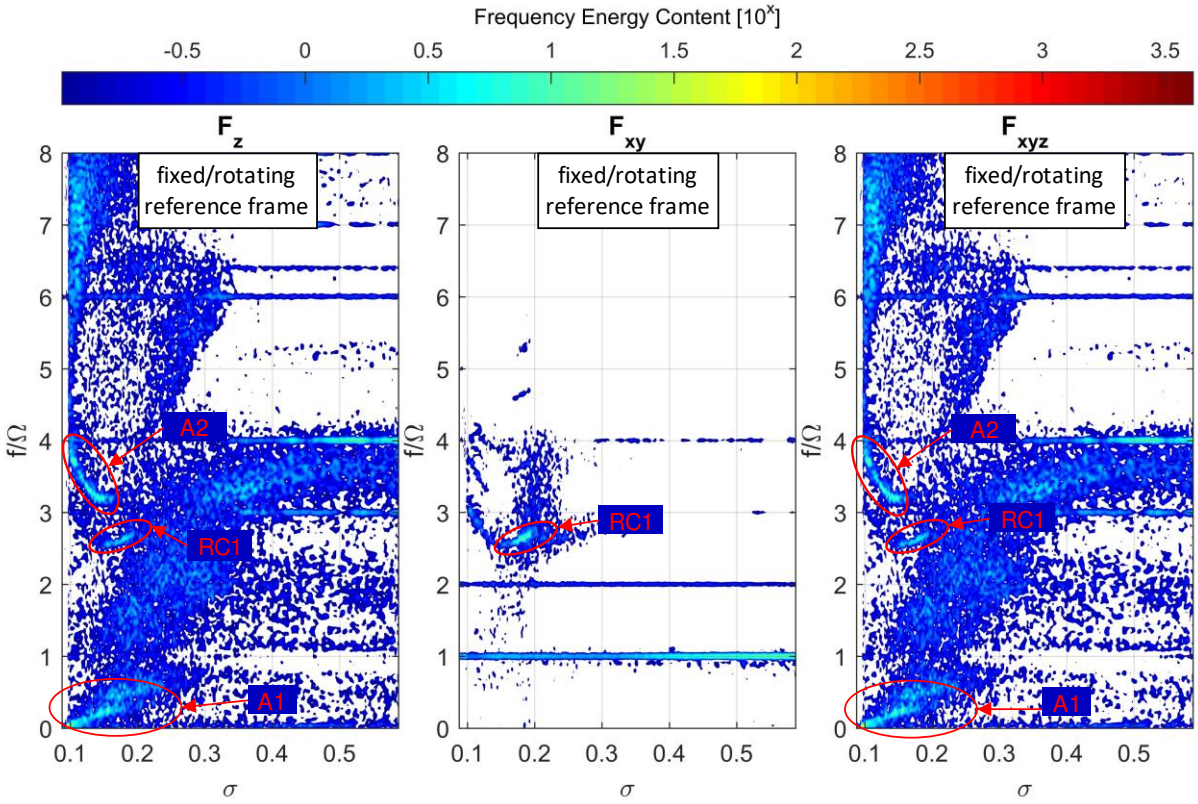

Figure 13. Frequency energy content $[N^2 \cdot s]$ of the force along the axis (F_z), its perpendicular component (F_{xy}), and the total force (F_{xyz}) acting on the dynamometer.

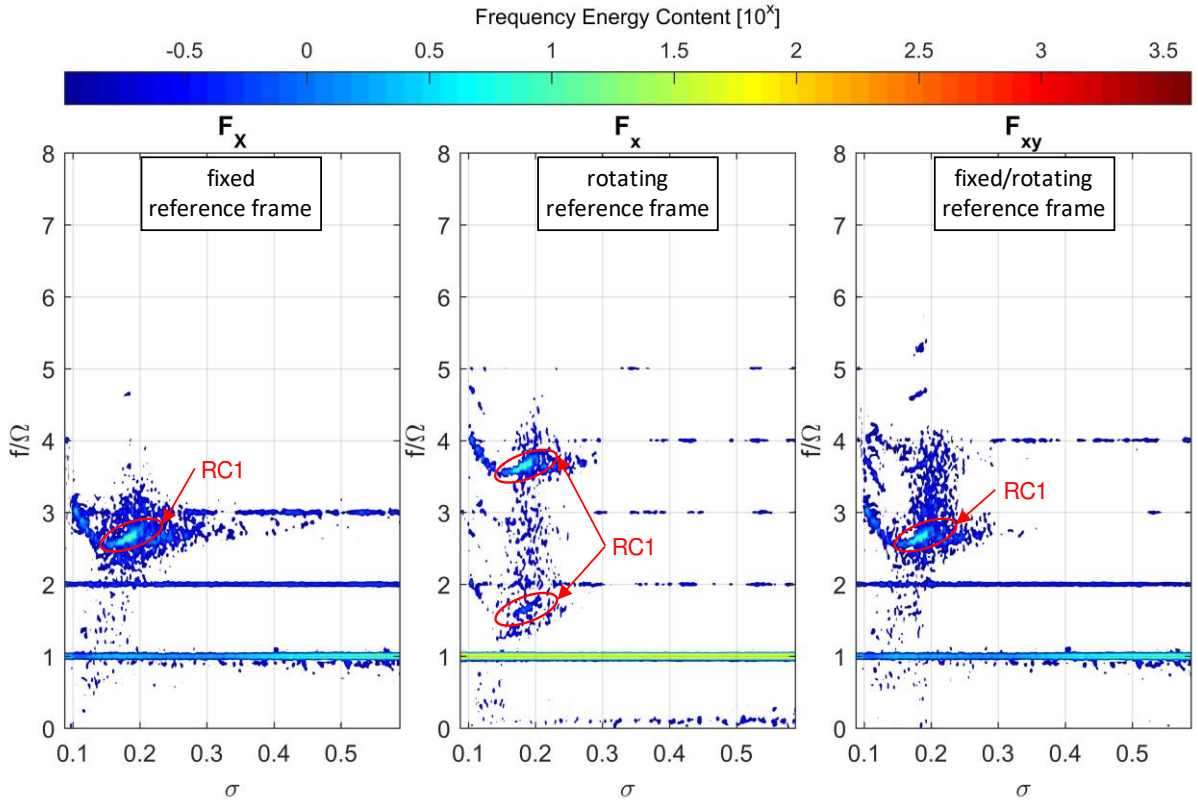

Figure 14. Frequency energy content $[N^2 \cdot s]$ of the force component along the X-axis in the absolute fixed reference frame (F_X, left), along the x-axis in the rotating reference frame (F_x) and its perpendicular component (F_{xy})acting on the dynamometer.

3 CONCLUSIONS

The experimental characterization of pressure fluctuations on a centrifugal pump for various operating regimes has been here presented and discussed. The paper focuses on the unsteady forces acting on the driving shaft which are triggered by such fluctuations. Although the paper presents data coming from a specific regime in terms of flow coefficient ($\Phi = 0.9\Phi_D$), similar behaviors have been detected for analogous phenomena observed during other regimes. In particular, the presence of rotating phenomena may generate fluctuations of the force in the plane perpendicular to the rotational axis as well as on the rotational axis itself. On the perpendicular plane, the frequency content associated with the generated force suggests that the force can be approximated by the sum of a component with a fixed direction and fluctuating intensity together with a purely rotating component. The frequency of both components is the same as for the source phenomenon. A key role in such behavior is most likely played by the single-tongue volute whose intrinsic asymmetry interacts with the rotating phenomena leading to force amplitude fluctuations. At $\Phi = \Phi_D$ the outlet flow has a nominal zero incidence angle with the tongue, which is most likely the reason why the force triggered by cavitation instabilities is also reduced. Thus, confirming the goodness of the pump design approach described in [25]. However, experimental campaigns are needed to better understand the interaction between the presence of cavitation instabilities and forces in presence of different shaped volutes and diffusers. Furthermore, the paper highlights that special attention should be paid when the pump design includes any stator (e.g. a vaned diffuser) especially when the operating conditions may include cavitation.

On the other hand, axial phenomena lead to fluctuations of the force component directed along the rotational axis only.

To date, it is not clear which eventual unstable forces would arise with an inducer ahead of a centrifugal stage (typical in space application) under the presence of cavitation instabilities. However, the present results suggest that the massive presence of such instabilities for an inducer (if compared to a centrifugal stage) may lead to possible dangerous conditions when the inducer is coupled with static elements typical of centrifugal stages (e.g. the volute tongue). Further investigations are needed in order to better clarify these aspects.

4 NOMENCLATURE

Latin

A	Axial
A_f	Fluctuation amplitude
E_f	Fluctuation energy
$\tilde{F}$	Force intensity fluctuation
F	Force
N	Blade Number
Q	Volumetric Flow Rate
RC	Rotating Cavitation
Re	Reynolds
S	Power Spectrum Density
T	Temperature
f	frequency
n	Flow instability lobes
p	Pressure
r	Radius
z	Axial Length, rotating axis

Greek

Δ	Variation
Φ	Flow Coefficient
Ψ	Head Coefficient
Ω	Rotational Speed
γ_{xy}	Coherence between sensors x and y
ν	Fluid Kinematic Viscosity
ρ	Fluid Density
σ	cavitation number
ω	Force angular frequency
φ	Cross-spectrum phase
θ	Force initial phase
ϑ	Azimuthal direction

Subscripts

D	Design
N	Nominal
T	Total
c	chamber
in	Inlet
v	vapor
xyz	Rotating frame
XYZ	Fixed frame

5 ACKNOWLEDGMENTS

The present work has been possible thanks to the supports of the European Space Agency along several years. The authors would like to express their great gratitude to Dr. Giorgio Saccoccia and to Dr. Gianni Pellegrini. Special gratitude goes to Lucio Torre that has been a great mainstay of the whole Chemical Propulsion Team for many years and to Dr. A. Sonaho (now GMYS-Space).

6 REFERENCES

[1] A. Bhattacharyya, A. J. Acosta, C. E. Brennen and T. K. Caughey, "Rotordynamic Forces in Cavitating Inducers," *J. Fluids Eng.,* vol. 119, no. 4, pp. 768-774, 1997.

[2] A. Bhattacharyya, "Internal Flows and Force Matrices in Axial Flow Inducers," California Institute of Technology, Pasadena, 1994.

[3] R. Franz, "Experimental investigation of the effect of cavitation on the rotordynamic forces on a whirling centrifugal pump impeller," California Institute of Technology, Pasadena, 1989.

[4] W. Rosenmann, "Experimental Investigations of Hydrodynamically Induced Shaft Forces With a Three Bladed Inducer," in *ASME Symp. on Cavitation in Fluid Machinery*, 1965.

[5] F. Ehrich and S. D. Childs, "Self-Excited Vibrations in High Performance Turbomachinery," *Mechanical Engineering,* pp. 66-79, 1984.

[6] P. Hergt and P. Krieger, "Paper 10: Radial Forces in Centrifugal Pumps with Guide Vanes," in *Proceedings of the Institution of Mechanical Engineers*, 1969.

[7] T. Suzuki, R. Prunieres, H. Horiguchi, T. Tsukiya, Y. Taenaka and T. Y., "Measurements of Rotordynamic Forces on an Artificial Heart Pump Impeller," *J. Fluids Eng.,* vol. 129, no. 11, pp. 1422-1427, 1 November 2007.

[8] C. E. Brennen, R. Franz and N. and Arndt, "Effects of Cavitation on Rotordynamic Force Matrices," in *3rd Earth to Orbit Propulsion Conf.*, Huntsville, AL, USA, 1988.

[9] T. Hashimoto, H. Yoshida, M. Watanabe, K. Kamijo and Y. Tsujimoto, "Experimental Study on Rotating Cavitation of Rocket Propellant Pump Inducers," *Journal of Propulsion and Power,* vol. 13, no. 4, pp. 488-494, July-August 1997.

[10] Y. Tsujimoto, Y. Yoshida, Y. Maekawa and S. Watanabe, "Observation of Oscillating Cavitation of an Inducers," *ASME J. Fluids Eng. ing,,* vol. 119, pp. 775-781, 1997.

[11] T. Zoladz, "Observations on Rotating Cavitation and Cavitation Surge from the Development of the Fastrac Engine Turbopump," in *36th AIAA/ASME/SAE/ASEE Joint Propulsion Conference*, Huntsville, AL, USA, 2000.

[12] Y. Tsujimoto and Y. A. Semenov, "New Types of Cavitation Instabilities in Inducers," in *4th Int. Conf. on Launcher Technology*, Liege, Belgium., 2002.

[13] M. Subbaraman and M. Patton, "Suppressing Higher-Order Cavitation Phenomena in Axial Inducers," in *CAV2006, 6th Int. Symposium on Cavitation*, Wageningen, The Netherlands, 2006.

[14] K. Kamijo, M. Yoshida and Y. Tsujimoto, "Hydraulic and Mechanical Performance of LE-7 LOX Pump Inducer," *J. Propulsion and Power,* vol. 9, no. 6, pp. 819-826, 1993.

[15] A. Cervone, L. Torre, C. Bramanti, E. Rapposelli and L. d'Agostino, "Experimental Characterization of Cavitation Instabilities in a Two-Bladed Axial Inducer," *AIAA Journal of Propulsion and Power,* vol. 22, no. 6, pp. 1389-1395, 2006.

[16] A. Cervone, L. Torre, A. Pasini and L. d'Agostino, "Cavitation and Flow Instabilities in a 3- Bladed Axial Inducer Designed by Means of a Reduced Order Analytical Model," in *Seventh International Symposium on Cavitation*, Ann Arbor, Michigan, USA, 2009.

[17] L. Torre, G. Pace, P. Miloro, A. Pasini, A. Cervone and L. d'Agostino, "Flow Instabilities on a Three-Bladed Axial Inducer at Variable Tip Clearance," in *13th Int. Symp. on Transport Phenomena and Dynamics of Rotating Machinery (ISROMAC-13)*, Honolulu, Hawaii, 2010.

[18] J. Friedrichs and G. Kosyna, "Rotating Cavitation in a Centrifugal Pump Impeller of Low Specific Speed," in *Prceedings of Fluids Engineering Division Summer Meeting, 4th International Symposium of Pumping Machinery*, New Orleans, Louisiana, May 29-June 1, 2001.

[19] K. Yamamoto, "Instability in a cavitating centrifugal pump," *JSME international journal Ser. 2. Fluids engineering, heat transfer, power, combustion, thermophysical properties,* vol. 34, pp. 9-17, 1991.

[20] D. Valentini, G. Pace, L. Torre, A. Pasini and L. d'Agostino, "Influences of the Operating Conditions on the Rotordynamic Forces Acting on a Three-Bladed Inducer Under Forced Whirl Motion," *J. Fluids Eng,* vol. 137, no. 7, p. 071304, 01 July 2015.

[21] D. Valentini, G. Pace, A. Pasini, R. Hadavandi and L. d'Agostino, "Fluid-Induced Rotordynamic Forces on a Whirling Centrifugal Pump," in *ISROMAC XVI*, Honolulu, HI, 2016.

[22] D. Valentini, G. Pace, L. Torre, A. Pasini and L. d'Agostino, "Pumping and Suction Performance of a Whirling Inducer," in *Space Propulsion 2014*, Cologne, Germany, 19-22 May 2014.

[23] G. Pace, A. Pasini, L. Torre, D. Valentini and L. d'Agostino, "The Cavitating Pump Rotordynamic Test Facility at ALTA S.p.A.: Upgraded Capabilities of a Unique Test Rig," in *Space Propulsion Conference*, Boredeaux, France, 2012.

[24] L. d'Agostino, "Comparison of rotordynamic fluid forces in axial inducers and centrifugal turbopump impellers," in *IOP Conference Series: Materials Science and Engineering*, 2016.

[25] L. d'Agostino, L. Torre, A. Pasini and A. Cervone, "A Reduced Order Model for Preliminary Design and Performance Prediction of Tapered Inducer," in *12th International Symposium on Trasport Phenomena*

and Dynamics of Rotating Machinery (ISROMAC-12), Honolulu, Hawaii, USA, 2008.

[26] L. d'Agostino, L. Torre, A. Pasini and A. Cervone, "On the Preliminary Design and Noncavitating Performance of Tapered Axial Inducers," *Journal of Fluids Engineering,* vol. 130, no. 11, 2008.

[27] D. Valentini, A. Pasini, P. G., L. Torre and L. d'Agostino, "Experimental Validation of a Reduced Order for Radial Turbopump Design," in *49th AIAA/ASME/SAE/ASEE Joint Propulsion Conference*, San Jose, California, USA, 2013.

[28] L. Torre, G. Pace, P. Miloro, A. Pasini, A. Cervone and L. d'Agostino, "Flow Instabilities on a Three-Bladed Axial Inducer at Variable Tip Clearance," in *13th Int. Symp. on Transport Phenomena and Dynamics of Rotating Machinery (ISROMAC-13)*, Honolulu, Hawaii, 2010.

[29] J. S. Bendat and A. G. Piersol, Random Data: Analysis and Measurement Procedures, New York, 1971.

[30] C. E. Brennen, Hydrodynamics of Pumps, Concepts ETI, Inc. and Oxford University Press., 1994.

[31] A. Cervone, L. Torre, A. Pasini and L. d'Agostino, "Cavitation and Flow Instabilities in a 3- Bladed Axial Inducer Designed by Means of a Reduced Order Analytical Model," in *7th International Symposium on Cavitation, CAV2009*, Ann Arbor, Michigan, USA, 2009.